PNAS
www.pnas.org

Supplementary Information for

Stormier Southern Hemisphere induced by topography and ocean circulation

Tiffany A. Shaw, Osamu Miyawaki and Aaron Donohoe

Corresponding Author name.
E-mail: tas1@uchicago.edu

This PDF file includes:

Figs. S1 to S11 (not allowed for Brief Reports)
Tables S1 to S2 (not allowed for Brief Reports)

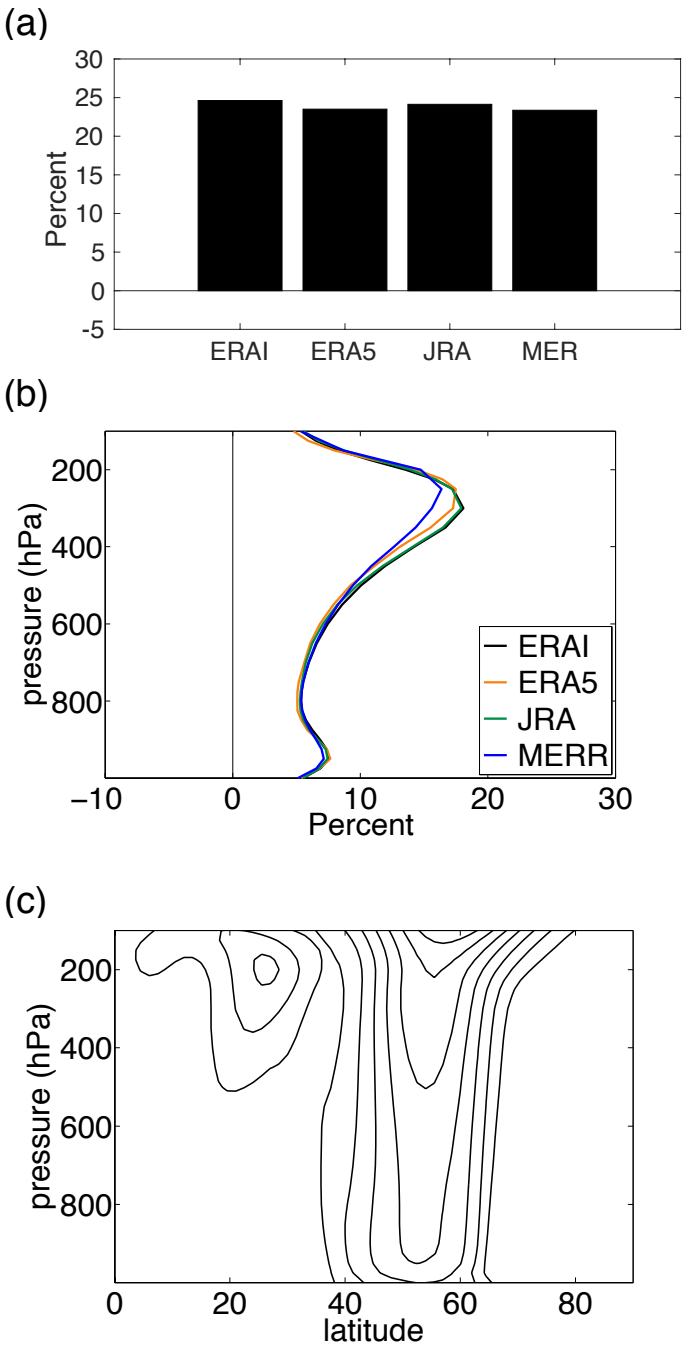

Fig. S1. Difference of Southern and Northern Hemisphere of (a) extratropical storminess (integrated across longitude and poleward of 20°), (b) storminess measured by transient eddy kinetic energy (averaged poleward of 20°) divided by the value at 250 hPa in the Northern Hemisphere and (c) longitudinal-mean zonal wind (1.5 ms^{-1} contour interval) averaged over reanalysis data sets.

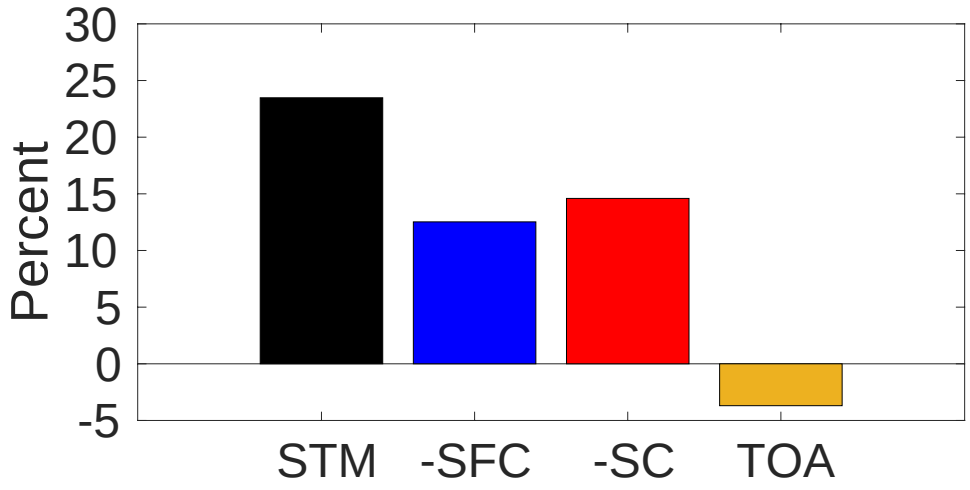

Fig. S2. Percentage difference of present-day storminess (difference of Southern and Northern Hemisphere divided by Northern Hemisphere) in ERA5 data from 1980 to 2018 for longitudinal-mean, vertically-integrated, latitudinally-integrated (poleward of 20°) transient eddy moist static energy flux (STM) decomposed into surface energy flux (SFC), stationary circulation (SC) and top-of-atmosphere (TOA) contributions.

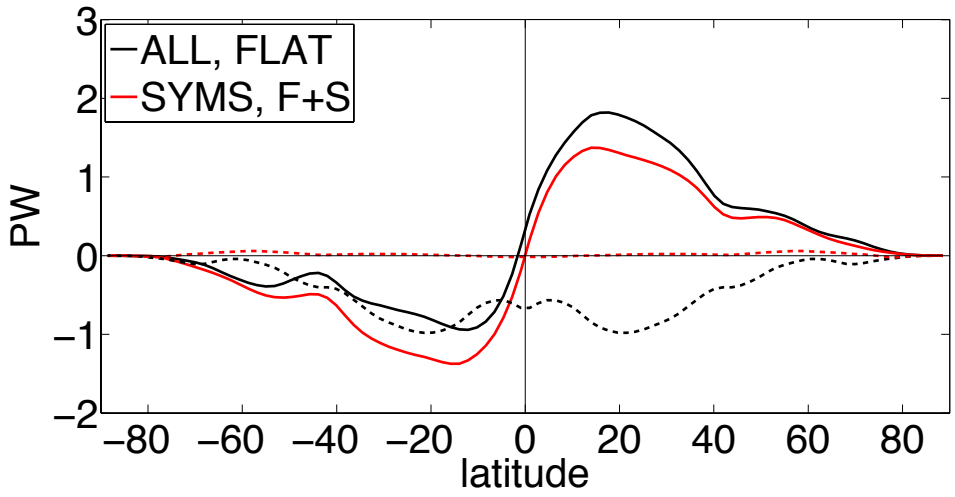

Fig. S3. Ocean energy transport inferred from imposed surface energy fluxes in ECHAM6 climate model simulations (solid lines) and hemispheric asymmetry (Southern Hemisphere minus Northern Hemisphere, dashed).

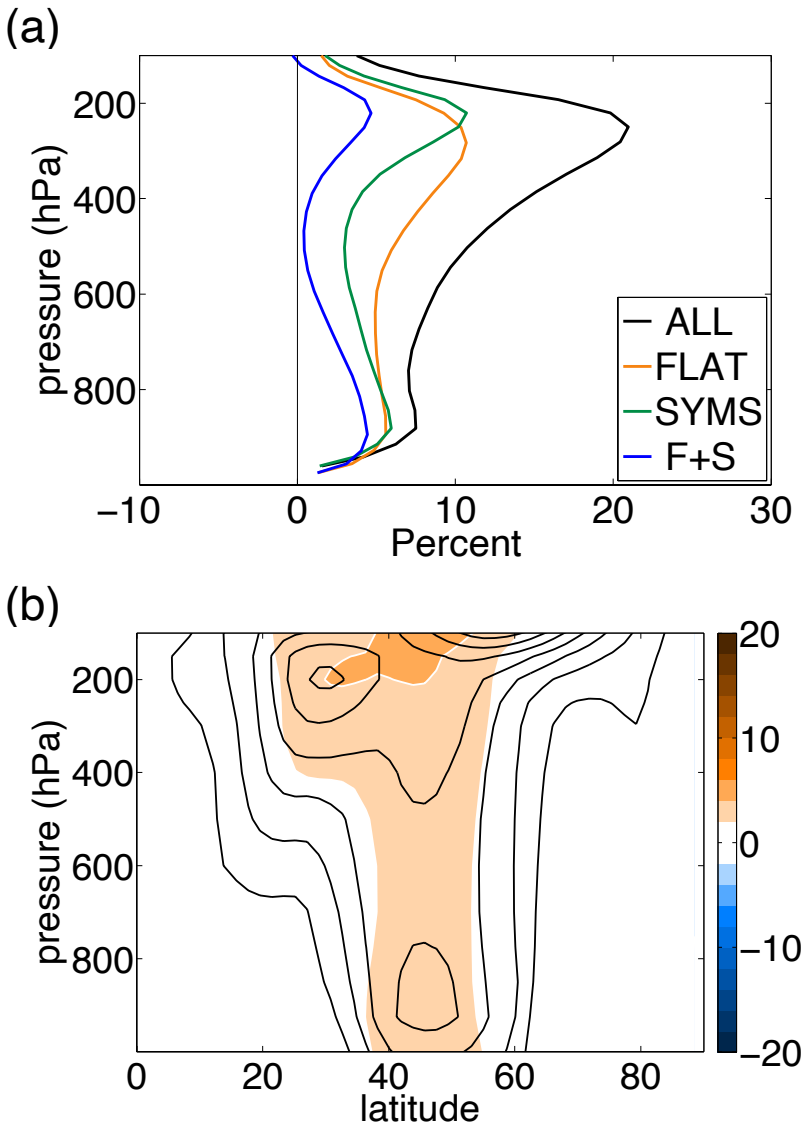

Fig. S4. Hemispheric asymmetry (difference of Southern and Northern Hemisphere) of (a) storminess measured by eddy kinetic energy divided by the value at 250 hPa for ECHAM6 climate model simulations and (b) longitudinal-mean zonal wind (1.5 ms^{-1} contour interval) for ALL (black) and F+S (colors).

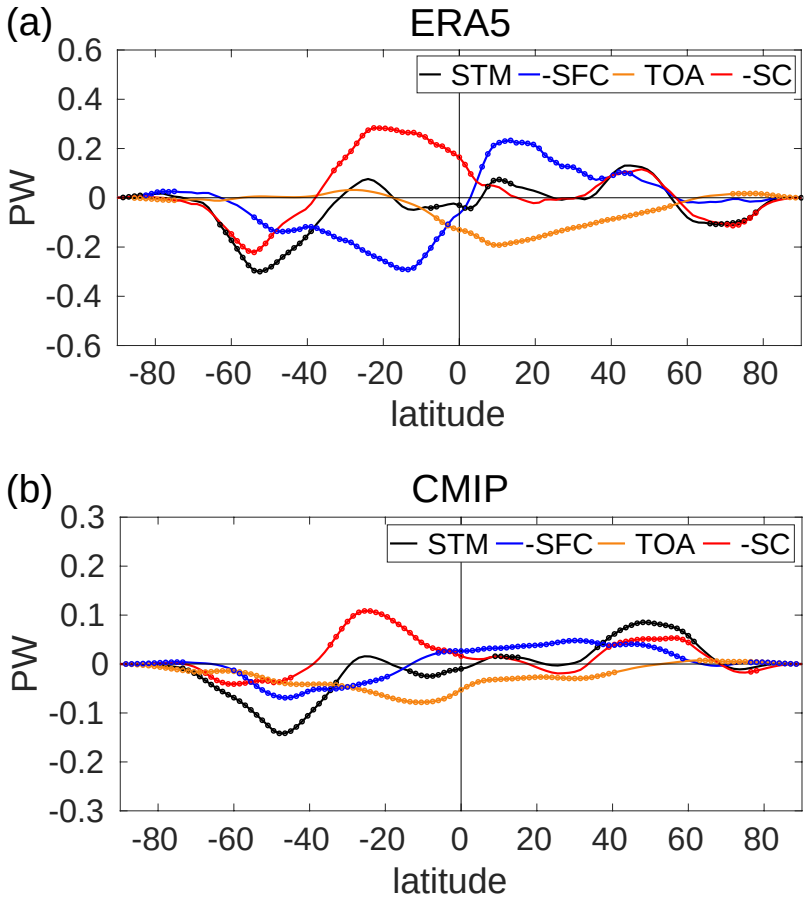

Fig. S5. Trend of eddy MSE flux storminess (STM) from 1980 to 2018 decomposed into contributions from surface energy fluxes (SFC), TOA radiative fluxes (TOA) and stationary atmospheric circulation energy fluxes (SC) in (a) ERA5 and (b) CMIP5. Trends that are statistically significant (p values lower than 0.05) are marked with a circle.

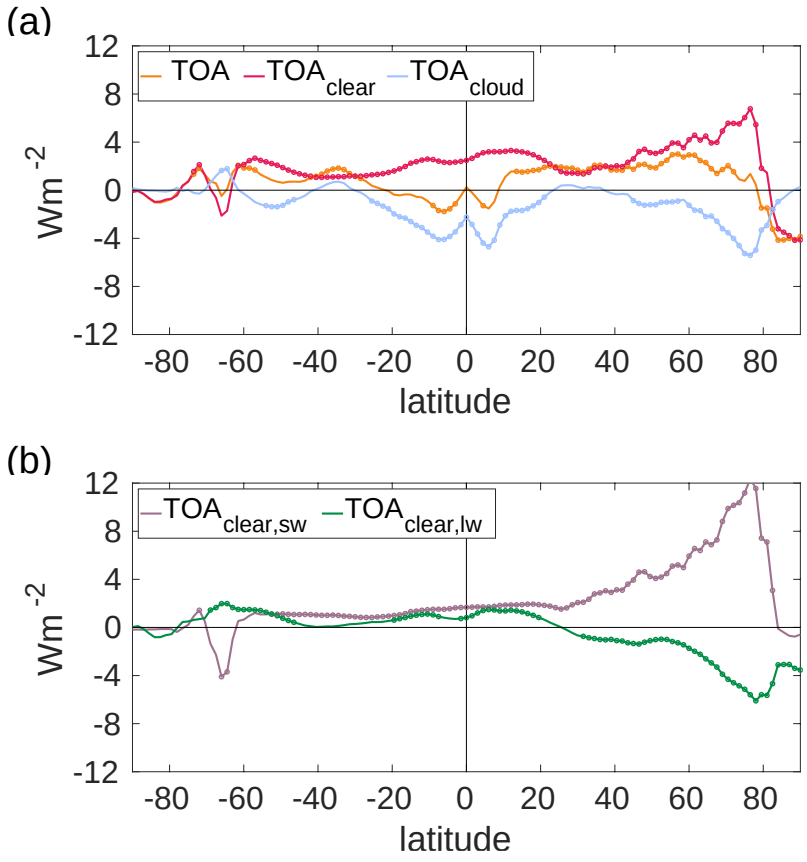

Fig. S6. (a) Trend of ERA5 TOA radiative fluxes from 1980 to 2018 decomposed into clear-sky and cloud-sky contributions. (b) Trend of ERA5 TOA clear-sky radiative fluxes from 1980 to 2018 decomposed into shortwave and longwave contributions. Trends that are statistically significant (p values lower than 0.05) are marked with a circle.

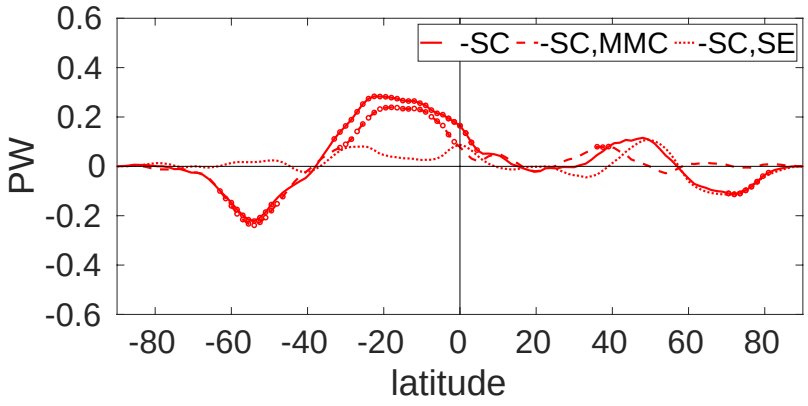

Fig. S7. Trend of ERA5 stationary atmospheric circulation energy fluxes (SC) decomposed into contributions from the mean meridional circulation (MMC, dashed) and stationary eddies (SE, dotted). Trends that are statistically significant (p values lower than 0.05) are marked with a circle.

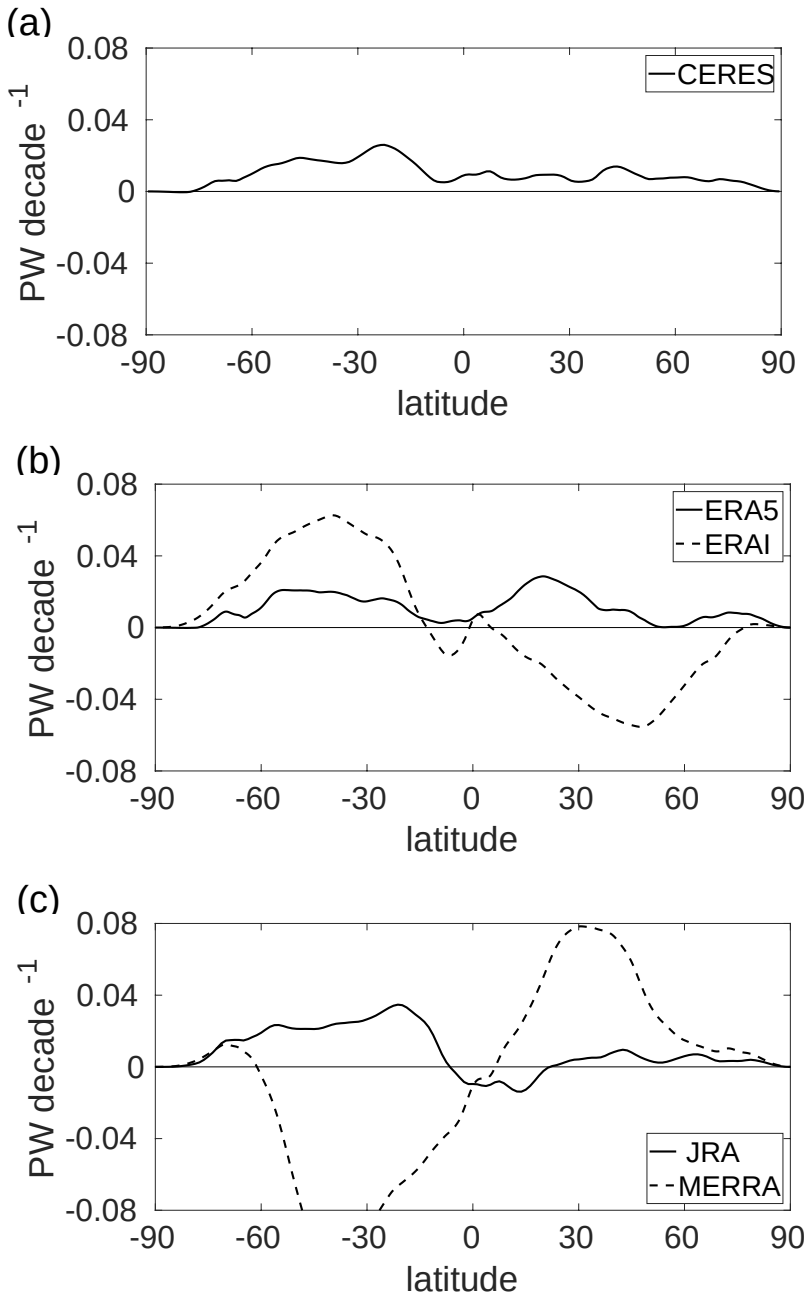

Fig. S8. Trend of energy flux implied from trends in TOA radiative energy fluxes from 2001 to 2018 for (a) CERES, (b) ERAI and ERA5, and (c) JRA55 and MERRA2 reanalysis data sets.

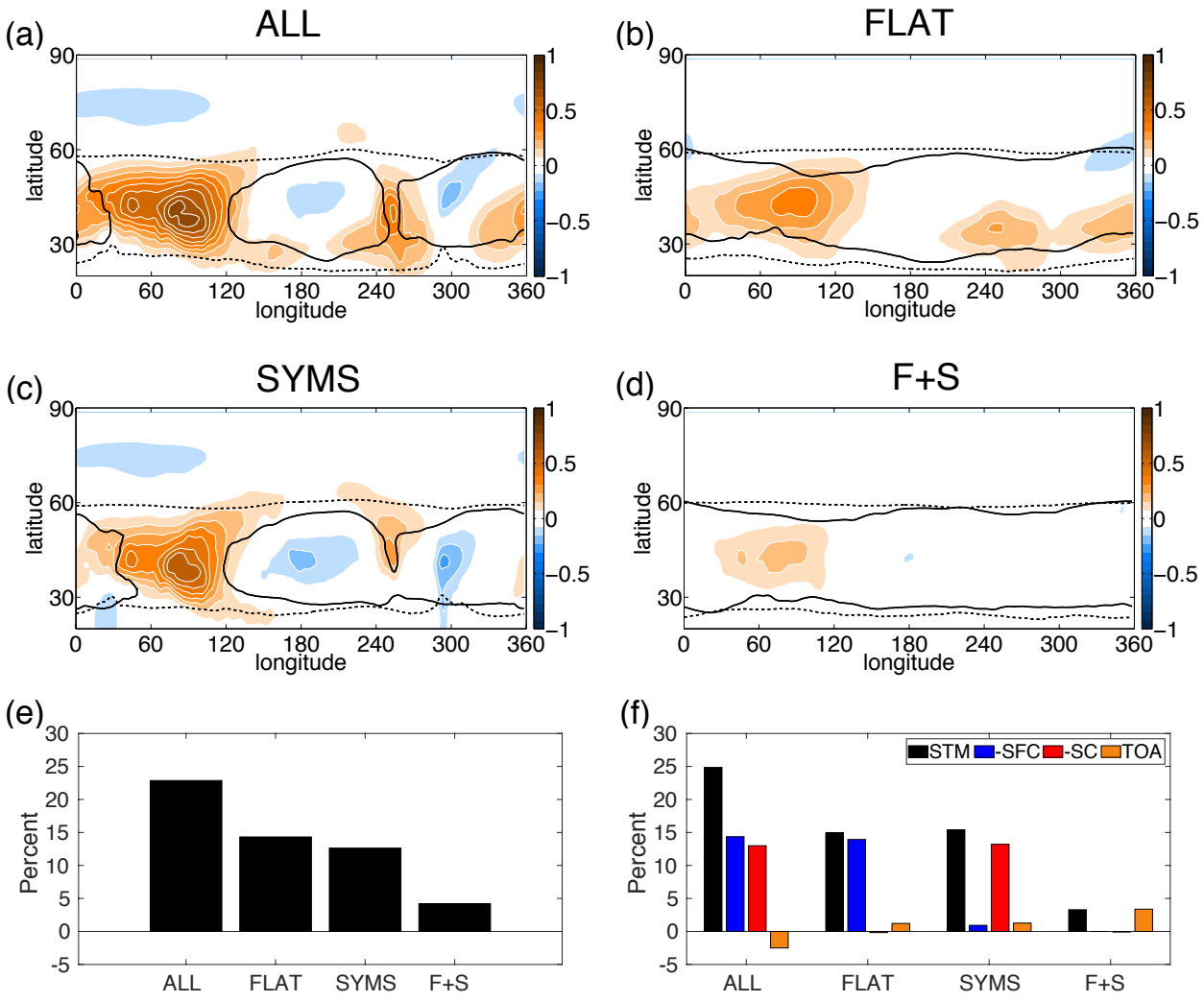

Fig. S9. Hemispheric asymmetry of storminess in climate model simulations with q-flux from an AMIP simulation. Hemispheric asymmetry of storminess (difference of Southern and Northern Hemisphere) as measured by vertically-integrated eddy kinetic energy (MJm^{-2}) for (a) climatology (ALL), (b) flattened topography (FLAT), (c) symmetrized surface energy fluxes (SYMS), and (d) flattened topography and symmetrized surface energy fluxes (F+S) simulations. Percentage difference of storminess (difference of Southern and Northern Hemisphere divided by Northern Hemisphere) across the simulations for longitudinal-mean, vertically-integrated, latitudinally-integrated (poleward of 20°) (e) eddy kinetic energy and (f) eddy moist static energy flux (STM) decomposed into surface energy flux (SFC), stationary circulation (SC) and top-of-atmosphere (TOA) contributions. The black lines in (a)-(d) indicate where storminess is equal to 0.6 MJm^{-2} for the Northern (solid) and Southern (dashed) hemispheres.

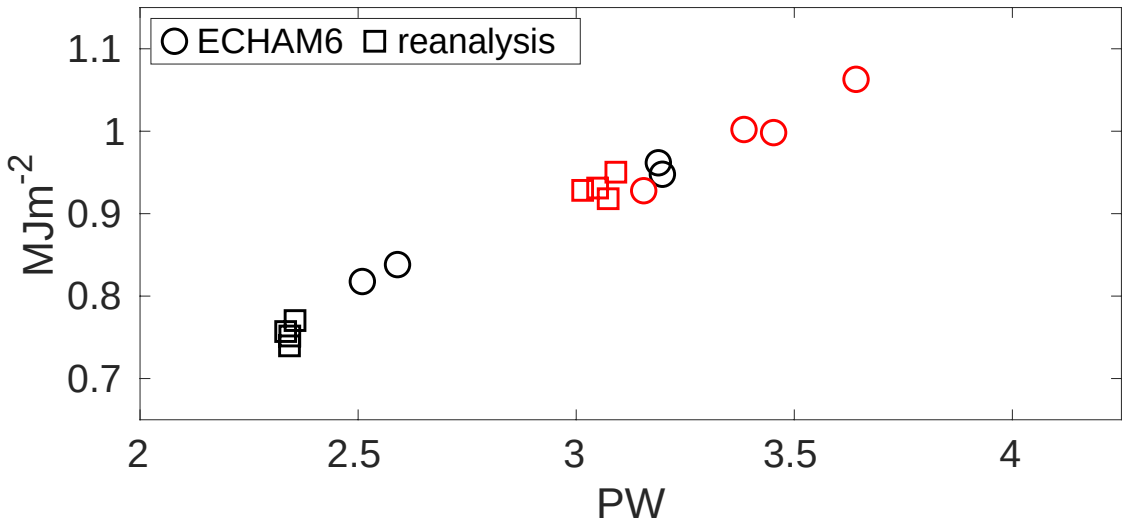

Fig. S10. Eddy kinetic energy versus transient eddy MSE flux for ECHAM6 simulations (circle) and reanalysis data (square) averaged over the extratropics (20-90°) of the Northern Hemisphere (black and Southern Hemisphere (red).

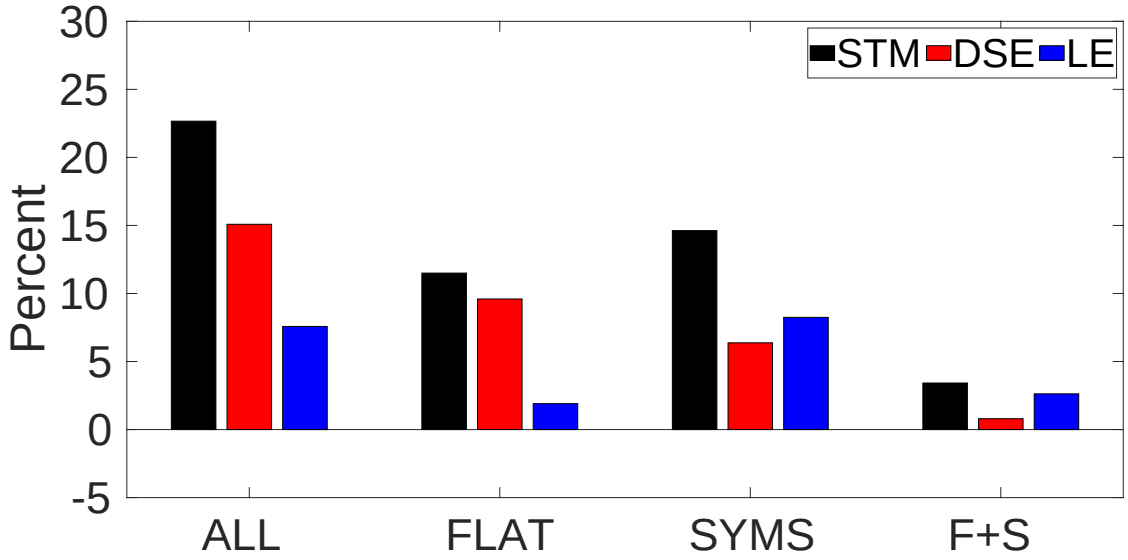

Fig. S11. Percentage difference of storminess (difference of Southern and Northern Hemisphere divided by Northern Hemisphere) across the simulations for longitudinal-mean, vertically-integrated, latitudinally-integrated (poleward of 20°) eddy moist static energy flux (STM, black) decomposed into dry static energy (DSE, red) and latent energy (LE, blue) contributions.

Table S1. Trends of storminess (MJm^{-2}) from 1980 to 2018 in the Northern (NH) and Southern (SH) Hemispheres across different data sets. The star indicates trends with p values lower than 0.05.

Data set	$EKE\ NH$	$EKE\ SH$
ERAI	0.0036	0.0229*
ERA5	0.0206	0.0421*
JRA55	-0.0040	0.0293*
MERRA2	-0.0025	0.0219*
CMIP5	0.0043	0.0109*
CMIP5 (2061-99)	0.0314*	0.0325*

Table S2. CMIP5 models analyzed in this study.

Model	*realization*
ACCESS1-3	r1i1p1
bcc-csm1-1	r1i1p1
bcc-csm1-1-m	r1i1p1
BNU-ESM	r1i1p1
CanESM2	r1i1p1
CCSM4	r1i1p1
CMCC-CESM	r1i1p1
CMCC-CM	r1i1p1
CMCC-CMS	r1i1p1
CNRM-CM5	r1i1p1
CSIRO-Mk3-6-0	r1i1p1
GFDL-CM3	r1i1p1
GFDL-ESM2G	r1i1p1
GFDL-ESM2M	r1i1p1
IPSL-CM5A-LR	r1i1p1
MIROC-ESM	r1i1p1
MIROC-ESM-CHEM	r1i1p1
MIROC5	r1i1p1
MPI-ESM-LR	r1i1p1
MPI-ESM-MR	r1i1p1
MRI-ESM1	r1i1p1
NorESM1-M	r1i1p1